Structural Characterization of Ca^{2+}-ATPase-Bound Phospholamban in Lipid Bilayers by Solid-State Nuclear Magnetic Resonance (NMR) Spectroscopy[†,‡]

Karsten Seidel,[§] Ovidiu C. Andronesi,[§,||] Joachim Krebs,[§] Christian Griesinger,[§] Howard S. Young,[⊥] Stefan Becker,[*,§] and Marc Baldus[*,§]

Max-Planck-Institute for Biophysical Chemistry, 37070 Göttingen, Germany, and Department of Biochemistry, University of Alberta, Edmonton, Alberta T6G 2H7, Canada

Received December 11, 2007; Revised Manuscript Received February 8, 2008

ABSTRACT: Phospholamban (PLN) regulates cardiac contractility by modulation of sarco(endo)plasmic reticulum calcium ATPase (SERCA) activity. While PLN and SERCA1a, an isoform from skeletal muscle, have been structurally characterized in great detail, direct information about the conformation of PLN in complex with SERCA has been limited. We used solid-state NMR (ssNMR) spectroscopy to deduce structural properties of both the $A_{36}F_{41}A_{46}$ mutant (AFA-PLN) and wild-type PLN (WT-PLN) when bound to SERCA1a after reconstitution in a functional lipid bilayer environment. Chemical-shift assignments in all domains of AFA-PLN provide direct evidence for the presence of two terminal α helices connected by a linker region of reduced structural order that differs from previous findings on free PLN. ssNMR experiments on WT-PLN show no significant difference in binding compared to AFA-PLN and do not support the coexistence of a significantly populated dynamic state of PLN after formation of the PLN/SERCA complex. A combination of our spectroscopic data with biophysical and biochemical data using flexible protein–protein docking simulations provides a structural basis for understanding the interaction between PLN and SERCA1a.

Sarco(endo)plasmic reticulum Ca^{2+}-ATPase (SERCA)[1] is the rate-determining enzyme for Ca^{2+} removal from muscle cytoplasm, a process that facilitates the relaxation of myofibrils subsequent to contraction. Phospholamban (PLN) regulates cardiac contractility by modulating the activity of SERCA2a, the heart muscle SERCA isoform (*1, 2*). Regulatory dysfunction of PLN on SERCA2a has been identified as a cause of dilated cardiomyopathy, and alterations of PLN activity can have manifold influence on the progress of heart disease, making the PLN−SERCA complex an important target for therapeutic intervention (*3*).

SERCA is a membrane protein of ∼110 kDa molecular weight, existing in a number of highly conserved isoforms (*4*). The skeletal muscle isoform SERCA1a (994 amino acid residues) has been structurally and functionally characterized in great detail, including the structure determination of reaction intermediates (see, e.g., (*5–9*)). In particular, the structure of the Ca^{2+}-free E_2 intermediate of SERCA1a, to which PLN can bind, is known at high resolution from X-ray crystallography (*5, 10*).

PLN is a 52-residue protein, whose structure has been studied by a variety of biophysical techniques. In line with other methods, nuclear magnetic resonance (NMR) spectroscopy revealed a transmembrane helix and a mobile N-terminal domain with some differences in the secondary structure of monomeric PLN mutants (*11–14*). Wild-type PLN predominantly exists as a symmetric homopentamer with a pore-resembling core spanning the membrane (*15, 16*), where the cytoplasmic domains can associate with the lipid bilayer (*17*).

Thus far, detailed structural information obtained directly on PLN in complex with SERCA has been limited. The binding interface of PLN with SERCA1a or SERCA2a, regarding both the transmembrane and cytoplasmic domains of PLN, was described by mutagenesis screening of PLN (*18–20*) and SERCA (*21, 22*), as well as cross-linking studies (*23–28*). Magic-angle-spinning (MAS) ssNMR has been used to selectively probe internuclear distances in pairwise isotope-labeled PLN variants bound to SERCA1a (*29*), while, for example, EPR and FRET have been employed to study overall conformational changes upon complex formation (*30, 31*). Current models for the structure of PLN when bound to SERCA1a (E_2 state) were obtained from computational approaches using mutagenesis and cross-linking constraints for all domains of PLN (*26, 32*) or with a focus on the transmembrane region (*27, 28*). In these studies, the initial template structure of PLN for molecular modeling was taken from investigations of free PLN (*12, 33*). Solution-state NMR data obtained for AFA-PLN in the presence

[†] This work was supported by the Max Planck Society. H.S.Y. is supported by the Heart and Stroke Foundation of Canada and the Alberta Heritage Foundation for Medical Research.

[‡] The AFA-PLN/SERCA1a docking model coordinates can be obtained directly from the corresponding authors upon request.

* To whom correspondence should be addressed. Telephone: +49-551-201-2222. Fax: +49-551-201-2202. E-mail: sabe@nmr.mpibpc.mpg.de (S.B.); Telephone: +49-551-201-2212. Fax: +49-551-201-2202. E-mail: maba@mpibpc.mpg.de (M.B.).

[§] Max-Planck-Institute for Biophysical Chemistry.

[||] Present address: Martinos Center for Biomedical Imaging, Massachusetts General Hospital, Harvard Medical School, Boston, MA 02114.

[⊥] University of Alberta.

[1] Abbreviations: SERCA, sarco(endo)plasmic Ca^{2+}-ATPase; PLN, phospholamban; NMR, nuclear magnetic resonance; ssNMR, solid-state NMR; MAS, magic angle spinning; SD, spin diffusion.

10.1021/bi7024194 CCC: $40.75 © 2008 American Chemical Society
Published on Web 03/21/2008

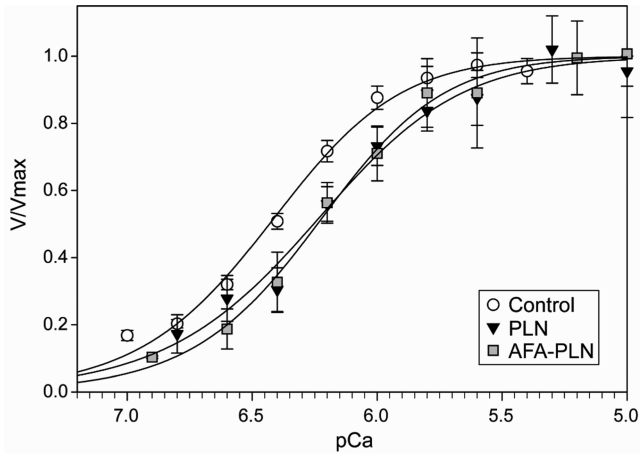

FIGURE 1: ATPase activity as a function of the free Ca^{2+} concentration for Ca^{2+}-ATPase reconstituted in the absence (circles) and presence of recombinant wild-type PLN (triangles) or AFA-PLN (squares). The raw data were normalized to the maximal activity calculated on the basis of fitting the data to the Hill equation (n = 5 for control, n = 4 for wild-type PLN, and n = 3 for AFA-PLN). The data are plotted as normalized ATPase activity versus pCa. Each data point is the mean ± standard error of the mean (SEM).

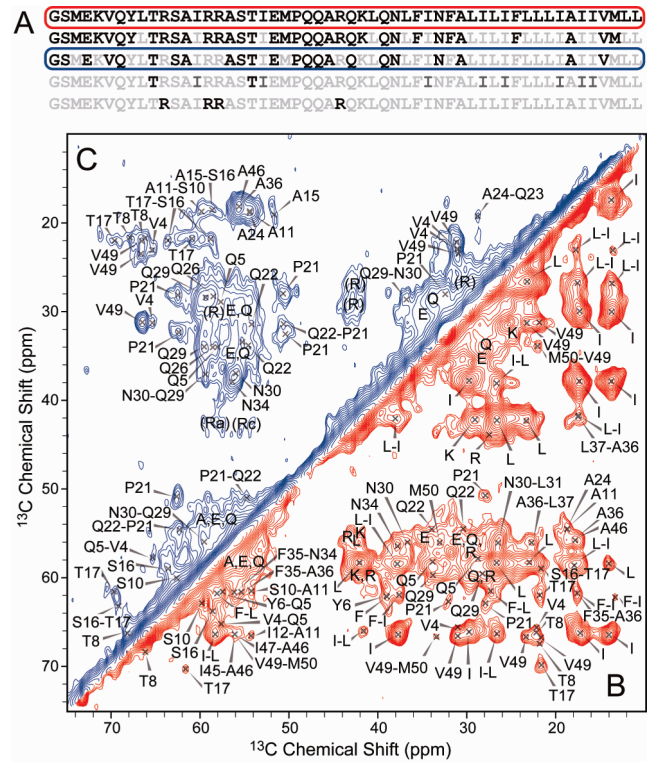

FIGURE 2: (A) Sequence of $A_{36}F_{41}A_{46}$-PLN used in this study. Labeled and unlabeled residues are given in black and light gray, respectively. (B and C) SDWC experiments conducted on U(^{13}C,^{15}N)-AFA-PLN/SERCA1a (B) and reverse-labeled U(^{13}C,^{15}N \ILRK-MYF)-AFA-PLN/SERCA1a (C) at a temperature of 266 and 235 K, respectively. See parts A and B of Figure S1 in the Supporting Information for full spectra.

of SERCA were interpreted in terms of two or more transient conformations that are present during the PLN−SERCA interaction, structurally different from results seen for free PLN in solution (*34*). Additionally, the existence of a transient WT-PLN intermediate during complex formation with SERCA was hypothesized on the basis of a structural model of the pentamer (*16*). However, these studies were conducted in micelles where complex formation and protein activity can be compromised (*34*) and did not provide direct spectroscopic information about PLN in complex with SERCA.

Significant progress has been achieved in monitoring structure, dynamics, and complex formation of multiply labeled proteins in lipid bilayers by ssNMR. Even if only low quantities of the molecule of interest are available, conformation-dependent chemical shifts (*35*) provide information on secondary structure (see, e.g., ref *36*). We have applied high-resolution MAS ssNMR spectroscopy to multiple (^{13}C,^{15}N)-labeled variants of AFA- and WT-PLN in complex with SERCA1a to (i) directly infer the backbone-binding mode of PLN in complex with SERCA in a functional bilayer environment, (ii) investigate the presence of any additional, dynamic PLN conformation in our preparations, and (iii) generate a structural model that is compatible with biochemical data.

EXPERIMENTAL PROCEDURES

Sample Preparation. Fully uniformly (U) (^{13}C,^{15}N)-labeled recombinant AFA-PLN was expressed in *Escherichia coli* grown on ^{13}C-glucose and ^{15}N NH_4Cl and purified as described (*37*). Skeletal muscle vesicles were prepared from rabbit hind leg (*38*), and the skeletal SR Ca^{2+}-ATPase (SERCA1a) was purified by Reactive-Red Sepharose affinity chromatography (*39*). Hydrated proteoliposomes were prepared with DOPC as described by Hughes et al. (*29*). For the reconstitution, the molar ratio of SERCA1a/PLN/DOPC was 1:1.2:160. Typically 22 mg of purified Ca^{2+}-ATPase protein was reconstituted with 1.5 mg of labeled PLN or AFA PLN. ATPase activity of the proteoliposomes was assayed by measuring the absorbance of NADH at 340 nm over time in a coupled-enzyme assay (Figure 1) as previously described (*40*). The activity was measured in the range of 0.1 to 10 μM free Ca^{2+}. Full pCa curves were measured for each co-reconstitution. The data for at least three co-reconstitutions were averaged. The activity of each co-reconstitution was matched to a control of Ca^{2+}-ATPase reconstituted in the absence of PLN or AFA-PLN that had been prepared at the same time.

The primary sequence composed of 54 residues (PLN with initial Gly-Ser because of the expression construct) is given in Figure 2A. Reversely, IL- and ILRKMYF-labeled PLN samples were obtained from adding amino acids of natural ^{13}C and ^{15}N isotope abundance to the expression medium at concentrations of 100 mg/L for each amino acid. In contrast to Ile, Leu, Lys, Tyr, and Phe, reverse labeling of Arg residues was not complete as judged by 2D (^{13}C,^{13}C) (Figure 2C) and 1D ^{15}N ssNMR (data not shown) experiments. Nevertheless, a significant reduction of the corresponding ssNMR signals facilitated the assignment process. In addition, amino-acid-specific labeling was obtained by adding ^{13}C- and/or ^{15}N-labeled amino acids to the natural isotope abundance growth medium.

Solid-State NMR Experiments and Analysis. Samples were packed in standard 4 mm ZrO_2 rotors with top spacer and Kel-F caps. Experiments were carried out on Avance and Avance II NMR spectrometers (Bruker Biospin, Germany) equipped with triple-resonance (^{1}H,^{13}C,^{15}N) wide- or standard-bore probes, at magnetic fields corresponding to 400, 600, and 800 MHz ^{1}H Larmor frequency. MAS up to $\omega_{rot}/2\pi$ = 12.5 kHz was performed, using low-temperature VT gas

chillers at temperatures ranging from 235 to 275 K. ^{13}C chemical shifts were referenced with adamantane as external secondary standard, calibrating the $^{13}CH_2$ resonance to 31.47 ppm.

Residue identification and sequential resonance assignments were made from a double-quantum/single-quantum (2Q/1Q) correlation spectrum employing SPC5 (*41*) recoupling and from 2D spectra with mixing units using proton-driven spin diffusion (PDSD) (*42, 43*) or spin diffusion under weak (C',C^{α}) coupling conditions (SDWC) (*44*). Additionally, NCOCX and NCACX correlation spectra (*45*) were recorded with SPECIFIC NCO or NCA cross-polarization transfer (*46*), followed by homonuclear ^{13}C PDSD or DARR (*47*) mixing. Mobile protein segments were probed by a combination of through-bond (^1H,^{13}C) INEPT (*48*) and (^{13}C,^{13}C) TOBSY (*49*) mixing, suppressing the signal from residues exhibiting little or no mobility (*11*). During dipolar and scalar-based correlation experiments, SPINAL64 (*50*) or GARP (*51*) proton decoupling was applied at 85 and 10 kHz, respectively. All but through-bond spectra were recorded with 5–7 days of signal averaging, and the spectrum in Figure 2C was recorded over 9 days.

Signal processing was carried out in XWinNMR 3.5 or Topspin 2.0 (Bruker Biospin, Germany), employing zero-filling and exponential line broadening or square-sine-bell apodization functions. Two-dimensional spectral analysis was performed in Sparky 3.110 (Goddard and Kneller, University of California, San Francisco, CA). Secondary chemical shifts $\Delta\Delta\delta = (\delta_{CA}^{exp} - \delta_{CA}^{av}) - (\delta_{CB}^{exp} - \delta_{CB}^{av})$ (*35*) were calculated using average chemical shifts from the BioMagResBank (*52*).

Modeling Using Flexible Protein–Protein Docking Simulation. Docking models of PLN in complex with SERCA1a were calculated using the crystallography and NMR system (CNS) (*53*) with protocols for high-ambiguity-driven biomolecular docking (HADDOCK) (*54*) on a multinode computer cluster. A linearly stretched, partially prefolded docking template structure for PLN was generated using a standard simulated annealing protocol in CNS and then docked to a structure for SERCA1a in the E_2 state, Protein Data Bank (PDB) (*55*) entry 2AGV (*10*). Both protein structures were initially separated by 150 Å in random orientations. Docking was driven by intermolecular distance constraints summarized in Table 1. For details, see the Supporting Information.

Over the course of the docking simulation, PLN was constrained to a helical backbone conformation for the residues discussed below and fully flexible elsewhere. Interface residues of SERCA were allowed to have flexible side chains or backbone during various stages of the docking. Other parts of SERCA remained rigid during the simulation.

RESULTS

SsNMR Assignments and Secondary Structure of Mutant PLN. We used one- and two-dimensional (^{13}C,^{13}C) and (^{13}C,^{15}N) solid-state NMR correlation experiments to determine NMR chemical shifts of (monomeric) AFA-PLN in complex with SERCA1a. To reduce spectral overlap and assignment ambiguities, studies were performed with fully and reverse-labeled AFA-PLN, as well as two samples with amino acid-selective labeling. Isotope-labeling schemes are displayed in Figure 2A.

Table 1: Cross-link Restraints Used for the Docking between AFA-PLN and SERCA1a[a]

PLN	SERCA	maximum distance (Å)	link type	reference
3	397′, 400′	15	Denny−Jaffe	*23*
$4C^{\beta}$	364′	3	artificial	potential binding groove (*26*)
$12C^{\beta}$	358′	3	artificial	potential binding groove (*26*)
$27C^{\beta}$	$321'C^{\beta}$	5	SS	*26*
27	328′	10	EMCS	*25*
30	318′	10	BMH	*24*
30	321′	7	Cu−Phe but no SS	*26*
30	328′	15	KMUS	*25*
31	317′	10	BMH	*27*
$49C^{\beta}$	$89'C^{\beta}$	5	SS and Cu−Phe	*26 and 28*
50	89′	10	BMH	*28*
52	89′	7	bBBr	*28*

[a] Additional ambiguous interaction restraints (AIRs), as described for use in HADDOCK (*54*), were used to enforce interface contacts, such as residues with known loss-of-function mutations (see the Supporting Information). Of these residues, the following were defined as "active", mandating an ambiguous interface contact: (SERCA1a) 89, 321, 802, 805, and 809 and (AFA-PLN) 2, 4, 7, 9, 12, 27, 31, 34, 35, 38, 41, 42, 45, 48, 49, and 52. Abbreviations: SS, disulphide bond; EMCS: *N*-(ϵ-maleimidocaproyloxy)succinimide ester; BMH, 1,6-bismaleimidohexane; Cu−Phe, Cu−phenanthroline; KMUS, *N*-(κ-maleimidoundecanoyloxy)sulfo-succinimide ester; bBBr, dibromobimane.

Residue-type spin systems were identified from 2D (^{13}C,^{13}C) correlation spectra using PDSD mixing and from a homonuclear ^{13}C 2Q/1Q correlation spectrum (see the Supporting Information). Sequence-specific resonance assignments were facilitated by analysis of 2D (^{13}C,^{13}C) correlations with 150 ms SDWC mixing (*44*), shown in parts B and C of Figure 2 for fully and reversely (\ILRKMYF) labeled AFA-PLN, respectively. Several correlations could be assigned directly from fully labeled AFA-PLN, such as those involving C^{δ} in P21 in all (^{13}C,^{13}C) spectra or $M50C^{\beta}-V49C^{\alpha}$ in (^{13}C,^{13}C) SDWC (Figure 2B and Figure S1A in the Supporting Information). The spectrum of fully labeled AFA-PLN, however, is dominated by intra- and inter-residue correlations involving Ile and Leu. Using reverse-labeling, a significant reduction of spectral overlap (Figure 2C) and assignment ambiguities in the primary sequence (Figure 2A) was achieved. For example, $Q5C^{\alpha}-V4C^{\alpha}$, $T17C^{\gamma 2}-S16^{\alpha/\beta}$, and $N30C^{\beta}-Q29C^{\alpha}$, and their cross-diagonal correlations could now unambiguously be identified (Figure 2C and Figure S1B in the Supporting Information). In addition, a sequential assignment for R13C′ was obtained from a 1D SPECIFIC NCO-edited ^{13}C spectrum for (^{13}C,^{15}N)-Arg-labeled AFA-PLN (Figure S3 in the Supporting Information). Spectroscopy of (^{13}C-Thr,^{15}N-Ile)-AFA-PLN assisted in resolving Thr resonances (Figure S4 in the Supporting Information). Assignments are in-line with 2D NCACX and NCOCX correlation spectra for uniformly labeled (U) AFA-PLN (parts D and E of Figure S2 in the Supporting Information); however, because of lower resolution, dispersion, and sensitivity in these spectra, the assignments were primarily obtained from the homonuclear carbon correlations.

Even without unambiguous sequence-specific residue identifications, many cross-peaks could be assigned to

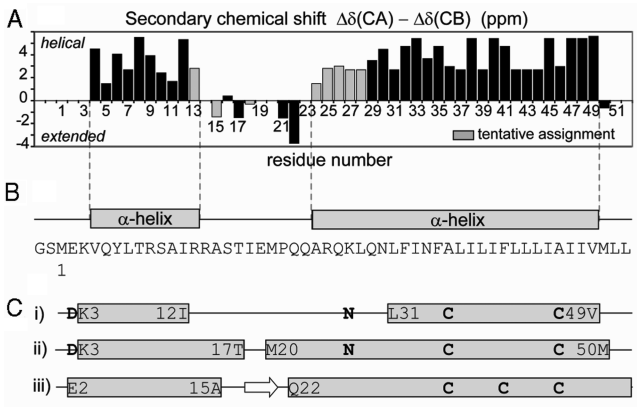

FIGURE 3: (A) Secondary-structure analysis of PLN bound to SERCA using ssNMR data and (B) the corresponding extent of a helical backbone indicated by gray boxes. (C) Comparison to previous models: (i) AFA-PLN/SERCA model by Toyoshima et al. (*26*), (ii) solution-state NMR results by Lamberth et al. (*12*) as used for the complex model by Hutter et al. (*32*), and (iii) WT-PLN in detergent micelles forming a pentamer (*16*), as discussed in context with rigid-body docking (*28*). In another pentamer model (not shown), the N-terminal helix further includes S16 (*17*). Mutants with respect to A are highlighted by bold letters.

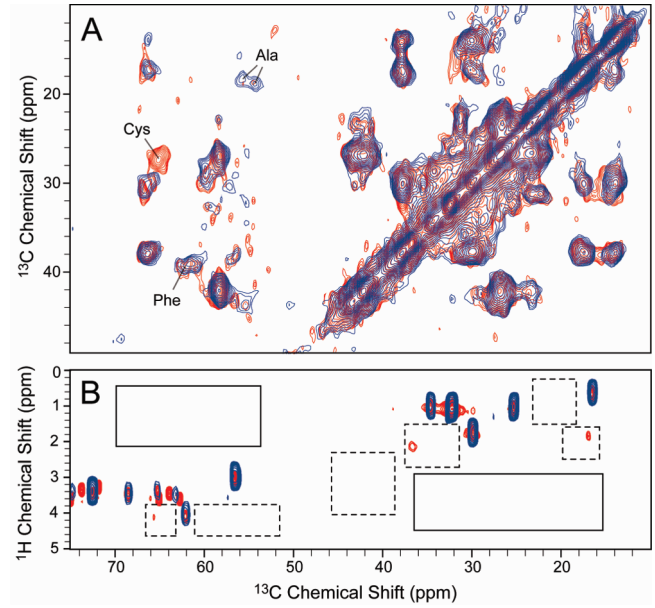

FIGURE 4: (A) Comparison of 2D (^{13}C,^{13}C) correlation spectra from 15 ms PDSD mixing for AFA-PLN (blue) and WT-PLN (red) (full spectra in Figures S5 in the Supporting Information). (B) Mobility-filtered (^{1}H,^{13}C) correlation spectrum from INEPT−TOBSY transfer of U-AFA-PLN/SERCA1a (blue) and INEPT transfer of U-WT-PLN/SERCA1a (red). Spectra were recorded with high-power SPINAL-64 or 10 kHz GARP decoupling in the case of AFA- and WT-PLN, respectively, resulting in different signal intensities for various lipid sites.

degenerate residue groups that occur exclusively within the same domain of AFA-PLN. This includes LI/IL pairs between L37 and I44, which give rise to numerous, strong sequential correlations (Figure 2B), or residues F32, F35, and F41 (see the Supporting Information for details). Met $C^{\alpha}-C^{\beta}$ chemical-shift correlations corresponding to a β strand (*56*) are not visible in the 2Q/1Q correlation spectrum, whereas the signal is detected for random-coil shifts (*56*), suggesting that there is no well-ordered β strand around M20 (*16*).

A qualitative separation of monomeric PLN segments exhibiting helical, extended, and coil backbone character was subsequently performed using secondary chemical-shift analysis. Backbone carbon resonances for V4, Q5, T8, and S10−R13 as well as Q29, N30, N34, V49, and nonspecifically assigned residues between F32 and I45 have helical character, whereas, for example, T17, Q22, and M50 show nonhelical propensities. In addition, we detected amino-acid-specific resonances of Ala (weak), Glu, Met, Ile, Ser, and Leu, corresponding to coil-like backbone structure (such as E2, A15, I18, and E19) and found Arg in different backbone configurations (Figure 2 and Figures S1−S4 in the Supporting Information). Because of signal overlap, Lys correlations indicative for a specific secondary structure could not be assigned.

When these findings are taken together, they suggest the existence of two helices comprising, at least, V4−R13 and Q29−V49, flanked by several residues of different backbone structure. Additional chemical shifts may be assigned to residues within helices that cannot be distinguished because of resonance overlap, such as Y6. Finally, taking into account earlier ssNMR distance measurements regarding A24C$^{\alpha}$−Q26N and the chemical shift of A24C$^{\alpha}$, indicating a helical backbone in this region (including R25), we could deduce a nonhelical linker range from R14 to Q22. Secondary chemical shifts of P21 and Q22 exclude continuation of the C-terminal α helix in these two residues. A summary of our secondary chemical-shift analysis for AFA-PLN in complex with SERCA1a is displayed in Figure 3A. Secondary chemical shifts indirectly depending upon previously published data for A24/Q26, as well as R13, depending upon R13C′ only, are colored gray.

Wild-Type PLN and PLN Mobility. To study whether structural differences previously seen between the AFA mutant and wild-type PLN are present in complex with SERCA, we conducted ssNMR experiments on a U(^{13}C,^{15}N)-WT-PLN/SERCA complex. Cysteine residues in WT-PLN gave rise to distinct (C^{α},C^{β}) correlations not observed in AFA-PLN in a (^{13}C,^{13}C) correlation spectrum with 15 ms PDSD mixing (Figure 4A and Figures S5 in the Supporting Information), corresponding to α-helical backbone conformation of the nonoxidized form. Ala (C^{α},C^{β}) cross-peaks were clearly diminished, owing to the absence of A36 and A46. While overall, the sample yields a lower signal-to-noise ratio, other cross-peaks appear identical at the given signal-to-noise level. In both spectra, recorded without freezing the samples, residues not buried in the membrane (e.g., M, E, Q, and R) give a rather weak signal, indicative of reduced structural order or increased mobility.

Protein segments exhibiting molecular motion in the micro- to nanosecond regime were probed by mobility-filtered INEPT or INEPT−TOBSY (^{1}H,^{13}C) correlation experiments (*11*) (Figure 4B). In contrast to free PLN, these spectra were devoid of typical protein correlations after one-bond H−C and additional ^{13}C−^{13}C transfer (dashed-framed and solid-framed boxes, respectively), as would be found for protein segments showing a high degree of mobility (*11*).

Docking Model. Next, we performed docking calculations to infer whether our spectroscopic data are compatible with previous biochemical studies. The five models with the best docking score are shown in Figure 5A. Close-up views for the best model, fulfilling all of the experimental constraints

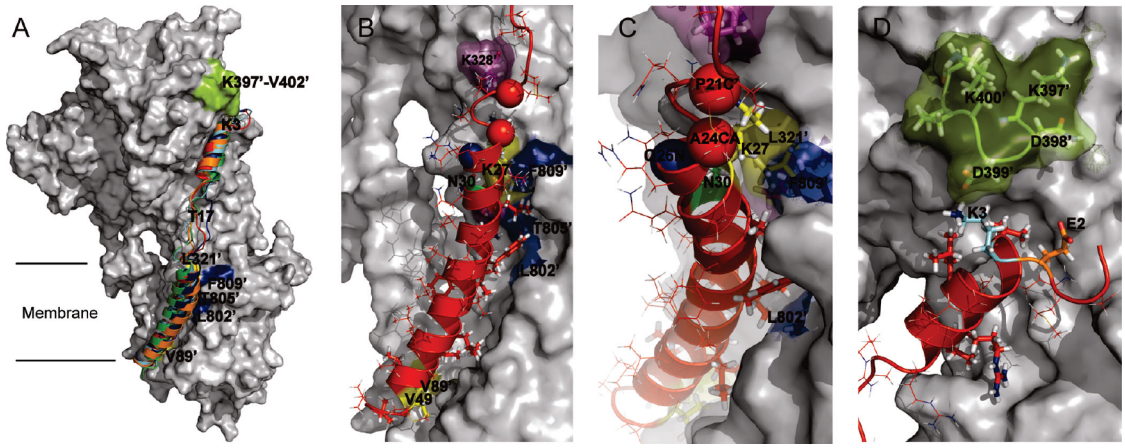

FIGURE 5: (A) Cluster of five conformations of AFA-PLN with the lowest docking score (cartoon) and SERCA1a (PDB ID 2AGV, gray surface). (B−D) Close-up views of the best scoring AFA-PLN conformer from A, for the C-terminal (B and C) and N-terminal (D) regions. SERCA residues that can be cross-linked with PLN by disulphide bonds (V89′ and L321′) are displayed as yellow patches; other cross-linked residues are displayed as magenta; residues 802′, 805′, and 809′ are shown in blue; and residues 397′–402′ are shown in green. Spheres indicate positions of specific isotope labels in an earlier ssNMR study (*29*). Residues of AFA-PLN and SERCA related to loss-of-function mutants and residues studied by chemical cross-linking are displayed as sticks, while other AFA-PLN residues are displayed as lines.

brought forward by ssNMR, cross-linking, and mutagenesis, are given in parts B−D of Figure 5.

Within the secondary-structure boundaries given by ssNMR, the N terminus of the cytoplasmic helix of AFA-PLN is found near the K397′−V402′ loop of SERCA1a (SERCA residues denoted with a prime), while the C terminus of the helix intimately connects to SERCA1a residues at the surface of transmembrane helices M4, M5, M6, and M9 (Figure 5). Residues 802′, 805′, and 809′, which exhibit loss-of-function mutations (*21*), are in contact with AFA-PLN (parts B and C of Figure 5). The distances between K27C$^{\beta}$ (AFA-PLN) and L321′C$^{\beta}$ as well as V49C$^{\beta}$ and V89′C$^{\beta}$ are compatible with the formation of disulphide cross-links of their respective cysteine mutants (*26–28*) (parts B and C of Figure 5). Furthermore, intramolecular AFA-PLN distances described by Hughes and Middleton (*29*) for A24C$^{\alpha}$−Q26N and P21C′−A24C$^{\alpha}$ (Table 1) are taken into account. Residues P21−Q23 form a loop allowing for dihedral angles compatible with Q22 backbone torsion-angle predictions from chemical shifts. The proximity of charged side chains E2 and K3 to K397′−V402′, as deduced from charge-altering mutations, leading to the loss of inhibitory function (*19, 22*), is fulfilled (Figure 5D).

DISCUSSION

Comparison to Previous Studies. Models of the PLN−SERCA complex have previously relied on structural data that was obtained for free PLN or deduced from biochemical data, such as mutagenesis and cross-linking. The corresponding secondary structures are given in Figure 3C and relate to (i) a model by Toyoshima and co-workers (*26*) based on two altered and computationally refined solution-state NMR structures for PLN (*12, 33*) and (ii) a model by Hutter et al. (*32*), which, during a docking simulation, enforced NOE constraints in solution for a free PLN monomer (*12*). As discussed in context of complex formation (*16, 28*), the secondary structure of WT-PLN pentamers seen by solution-state NMR spectroscopy in detergent micelles (*16*) is shown in Figure 3C (iii). Helix identifications from our ssNMR study are shown in Figure 3B, which points to differences in linker length in comparison to the previous studies.

In terms of the three-dimensional PLN/SERCA complex, our model differs substantially from earlier results by Hutter and co-workers (*32*). In their model, the C-terminal domain is shifted toward the cytosol. Instead, the membrane-spanning helix ends close to the SR luminal side of the lipid bilayer (parts A and B of Figure 5) based on the strong cross-link affinity of V49C to V89′C via a disulphide bridge (*26*) or Cu−Phe (*28*). Elsewhere, the position of the C-terminal helix in our model results from constraints derived from cross-links involving N30 and N27 (*25–27*), as well as the use of mutagenesis-derived AIRs. It is in-line with hydrogen-exchange measurements, which indicate that L44 is buried within the membrane (*29*). Furthermore, the secondary structure of AFA-PLN in our model was directly obtained from the complex with SERCA1a and not enforced to comply with the experimental NMR constraints on the structure of PLN alone (*12*), alleviating restraints on almost two full helix turns compared to free PLN.

Our docking model shows a similarity to the model proposed by Toyoshima and MacLennan (*26*). For the C terminus (Figure 5B), both models reflect the formation of a disulphide bond between V49C/V89′C double mutants and describe the absence of a helical backbone structure for AFA-PLN residues L51 and L52. Unwinding of the helix at V49, however, is not in agreement with our spectroscopic results and the resulting model. Furthermore, the C-terminal helix extends beyond L31, including N30 and Q29 (Figures 3 and 4B). Still, residue positions are in-line with the K27C−L321′C disulphide bond (*26*) and recently derived cross-linking constraints (*24, 25, 27, 28*). In addition, our model is compatible with the finding that A24 and Q26 are part of the helix (*29*) and incorporates the P21C′−A24C$^{\alpha}$ and A24C$^{\alpha}$−Q26N distances (*29*). Despite a longer C-terminal helix, we were also able to dock the cytoplasmic domain of AFA-PLN to residues in a pocket below the K397′−V402′ SERCA1a loop. K3 is found within 15 Å of K397′−K400′ (*23*), and proximity of E2 and K3 to K397′−V402′ may

facilitate interactions (Figure 5D). Residues exhibiting loss-of-function mutants are in contact with SERCA1a in both models.

Along with chemical cross-linking studies (*25, 27, 28*), rigid-body docking based on free PLN was to align the transmembrane helix with the structure of SERCA1a, raising the question if PLN K3 could reach near SERCA K397′−V402′ at all. Our results demonstrate that AFA-PLN computationally docked to the E_2 state of SERCA1a does satisfy the aforementioned interface constraints, when structural changes upon binding, facilitated by protein flexibility in the simulation, are taken into account. In addition, the SERCA structure in complex with PLN may differ from our docking template (PDB entry 2AGV). However, changes such as seen in crystal structures obtained using different or no inhibitors (*57, 58*) could be adapted by small structural alterations of PLN in our model.

Implications for Complex Formation and Phosphorylation. The secondary structure of AFA-PLN in complex with SERCA1a (parts A and B of Figure 3) implies a loss of secondary structure for several residues in the linker region compared to free AFA-PLN (*12, 14*) and to a lesser extent WT-PLN (*16*) (Figure 3C). In light of our structural model (Figure 5), this conformational flexibility is required for adaptation to the transmembrane and cytoplasmic SERCA binding sites. The existence of an extended linker already in the free WT form of PLN may be of advantage in complex formation. Indeed, the number of nonhelical linker residues of PLN in the complex is rather similar to WT-PLN (*16*) (iii in Figure 3C). However, this pentamer model cannot be docked to SERCA1a without violation of interface constraints or a structural rearrangement, as can be seen from manual docking using 3D visualization software (data not shown).

The importance of P21 to sustain unstructured characteristics in the segment preceding the C-terminal helix, providing conformational flexibility, has already been proposed from a structure determination of free PLN (*12*). An increase of helix propensity by P21A mutagenesis was found to reduce the ability of the N-terminal domain of PLN to efficiently inhibit SERCA1a (*59*). In fact, P21 does not only show chemical-shift characteristics of a statistical random-coil protein backbone but also bears an increase in ssNMR signal intensity when lowering the sample temperature (parts B and C of Figure 2 and Figure S1 in the Supporting Information), indicative of dynamic disorder in this protein segment. This notion further agrees with difficulties in assigning resonances from the linker segment in our 2D ssNMR data, because of unfavorable signal intensities or broadened resonance lines for these residues. Additional ssNMR experiments at elevated temperature could be used to further delineate the influence of structural and dynamic disorder and to potentially quantify the scale of motion for this segment. As noted earlier (*60*), this segment hosts the recognition sequence for phosphorylation by protein kinase A, which may be facilitated by local structural flexibility.

In summary, this study provides direct spectroscopic information on structural details of AFA- and WT-PLN in complex with SERCA1a in lipid bilayers. We identified for AFA-PLN in complex with SERCA a short N-terminal (V4−R13) and a long C-terminal (Q29−V49) helix intersected by a linker of reduced structural order from R14 to Q22. The C-terminal helix ends at V49. Our spectra corroborate an earlier site-specific observation that the C-terminal helix comprises residues A24−Q26 (*29*) but additionally show that P21 and Q22 do not constitute another helix turn. Two-dimensional correlation spectra recorded on WT-PLN in complex with SERCA1a exhibit no significant difference with respect to AFA-PLN. Mobility-filtered (^{1}H,^{13}C) correlation experiments speak against the existence of a significantly populated PLN conformation with dynamics on the micro- to nanosecond time scale after the formation of the complex. A combination of our spectroscopic results with biophysical and biochemical data using flexible protein–protein docking simulations leads to a structural model for AFA-PLN in complex with SERCA1a. While sharing similarities to the model by Toyoshima and co-workers, our model demonstrates that the extended length of the C-terminal α helix, obtained from experimental data, does not violate N-terminal binding near K397′−V402′ and takes into account recent cross-linking results. Furthermore, structural differences seen in the transmembrane helix and the potential influence of protein flexibility around the phosphorylation sequence may provide an important starting point for a more detailed analysis of protein–protein recognition and the regulatory effect of protein kinase A.

ACKNOWLEDGMENT

We gratefully thank Brigitta Angerstein, Kamila Sabagh, and Petra Widawka for assistance and Dr. Catharine Trieber (University of Alberta) for continuous help and support. Computational resources were provided by Gesellschaft für Wissenschaftliche Datenverarbeitung mbH Göttingen.

SUPPORTING INFORMATION AVAILABLE

Detailed description of the docking simulation, supplementary spectra for spectral assignments (Figures S1–S4), full spectra for the comparison of mutant and wild-type PLN (Figure S5), and docking templates and HADDOCK interface residues (Figure S6). This material is available free of charge via the Internet at http://pubs.acs.org.

REFERENCES

1. Simmerman, H. K. B., and Jones, L. R. (1998) Phospholamban: Protein structure, mechanism of action, and role in cardiac function. *Physiol. Rev. 78*, 921–947.
2. Tada, M., Kirchberger, M. A., and Katz, A. M. (1975) Phosphorylation of a 22,000-dalton component of cardiac sarcoplasmic reticulum by adenosine 3′−5′-monophosphate-dependent protein kinase. *J. Biol. Chem. 250*, 2640–2647.
3. MacLennan, D. H., and Kranias, E. G. (2003) Phospholamban: A crucial regulator of cardiac contractility. *Nat. Rev. Mol. Cell Biol. 4*, 566–577.
4. Periasamy, M., and Kalyanasundaram, A. (2007) SERCA pump isoforms: Their role in calcium transport and disease. *Muscle Nerve 35*, 430–442.
5. Toyoshima, C., Nakasako, M., Nomura, H., and Ogawa, H. (2000) Crystal structure of the calcium pump of sarcoplasmic reticulum at 2.6 Å resolution. *Nature 405*, 647–655.
6. Sorensen, T. L.-M., Moller, J. V., and Nissen, P. (2004) Phosphoryl Transfer and Calcium Ion Occlusion in the Calcium Pump. *Science 304*, 1672–1675.
7. Olesen, C., Sorensen, T. L. M., Nielsen, R. C., Moller, J. V., and Nissen, P. (2004) Dephosphorylation of the calcium pump coupled to counterion occlusion. *Science 306*, 2251–2255.
8. Toyoshima, C., and Nomura, H. (2002) Structural changes in the calcium pump accompanying the dissociation of calcium. *Nature 418*, 605–611.

9. Toyoshima, C., and Mizutani, T. (2004) Crystal structure of the calcium pump with a bound ATP analogue. *Nature 430*, 529–535.
10. Obara, K., Miyashita, N., Xu, C., Toyoshima, L., Sugita, Y., Inesi, G., and Toyoshima, C. (2005) Structural role of countertransport revealed in Ca^{2+} pump crystal structure in the absence of Ca^{2+}. *Proc. Natl. Acad. Sci. U.S.A. 102*, 14489–14496.
11. Andronesi, O. C., Becker, S., Seidel, K., Heise, H., Young, H. S., and Baldus, M. (2005) Determination of membrane protein structure and dynamics by magic-angle-spinning solid-state NMR spectroscopy. *J. Am. Chem. Soc. 127*, 12965–12974.
12. Lamberth, S., Schmid, H., Muenchbach, M., Vorherr, T., Krebs, J., Carafoli, E., and Griesinger, C. (2000) NMR solution structure of phospholamban. *Helv. Chim. Acta 83*, 2141–2152.
13. Traaseth, N. J., Buffy, J. J., Zamoon, J., and Veglia, G. (2006) Structural dynamics and topology of phospholamban in oriented lipid bilayers using multidimensional solid-state NMR. *Biochemistry 45*, 13827–13834.
14. Zamoon, J., Mascioni, A., Thomas, D. D., and Veglia, G. (2003) NMR solution structure and topological orientation of monomeric phospholamban in dodecylphosphocholine micelles. *Biophys. J. 85*, 2589–2598.
15. Smith, S. O., Kawakami, T., Liu, W., Ziliox, M., and Aimoto, S. (2001) Helical structure of phospholamban in membrane bilayers. *J. Mol. Biol. 313*, 1139–1148.
16. Oxenoid, K., and Chou, J. J. (2005) The structure of phospholamban pentamer reveals a channel-like architecture in membranes. *Proc. Natl. Acad. Sci. U.S.A. 102*, 10870–10875.
17. Traaseth, N. J., Verardi, R., Torgersen, K. D., Karim, C. B., Thomas, D. D., and Veglia, G. (2007) Spectroscopic validation of the pentameric structure of phospholamban. *Proc. Natl. Acad. Sci. U.S.A. 104*, 14676–14681.
18. Kimura, Y., Kurzydlowski, K., Tada, M., and MacLennan, D. H. (1997) Phospholamban inhibitory function is activated by depolymerization. *J. Biol. Chem. 272*, 15061–15064.
19. Toyofuku, T., Kurzydlowski, K., Tada, M., and Maclennan, D. H. (1994) Amino acids Glu2 to Ile18 in the cytoplasmic domain of phospholamban are essential for functional association with the Ca^{2+}-ATPase of sarcoplasmic reticulum. *J. Biol. Chem. 269*, 3088–3094.
20. Kimura, Y., Asahi, M., Kurzydlowski, K., Tada, M., and MacLennan, D. H. (1998) Phospholamban domain Ib mutations influence functional interactions with the Ca^{2+}-ATPase isoform of cardiac sarcoplasmic reticulum. *J. Biol. Chem. 273*, 14238–14241.
21. Asahi, M., Kimura, Y., Kurzydlowski, R., Tada, M., and MacLennan, D. H. (1999) Transmembrane helix M6 in sarco(endo)plasmic reticulum Ca^{2+}-ATPase forms a functional interaction site with phospholamban—Evidence for physical, interactions at other sites. *J. Biol. Chem. 274*, 32855–32862.
22. Toyofuku, T., Kurzydlowski, K., Tada, M., and Maclennan, D. H. (1994) Amino-acids Lys-Asp-Asp-Lys-Pro-Val402 in the Ca^{2+}-ATPase of cardiac sarcoplasmic reticulum are critical for functional association with phospholamban. *J. Biol. Chem. 269*, 22929–22932.
23. James, P., Inui, M., Tada, M., Chiesi, M., and Carafoli, E. (1989) Nature and site of phospholamban regulation of the Ca^{2+} pump of sarcoplasmic reticulum. *Nature 342*, 90–92.
24. Jones, L. R., Cornea, R. L., and Chen, Z. H. (2002) Close proximity between residue 30 of phospholamban and cysteine 318 of the cardiac Ca^{2+} pump revealed by intermolecular thiol cross-linking. *J. Biol. Chem. 277*, 28319–28329.
25. Chen, Z. H., Stokes, S. L., Rice, W. J., and Jones, L. R. (2003) Spatial and dynamic interactions between phospholamban and the canine cardiac Ca^{2+} pump revealed with use of heterobifunctional cross-linking agents. *J. Biol. Chem. 278*, 48348–48356.
26. Toyoshima, C., Asahi, M., Sugita, Y., Khanna, R., Tsuda, T., and MacLennan, D. H. (2003) Modeling of the inhibitory interaction of phospholamban with the Ca^{2+} ATPase. *Proc. Natl. Acad. Sci. U.S.A. 100*, 467–472.
27. Chen, Z. H., Stokes, D. L., and Jones, L. R. (2005) Role of leucine 31 of phospholamban in structural and functional interactions with the Ca^{2+} pump of cardiac sarcoplasmic reticulum. *J. Biol. Chem. 280*, 10530–10539.
28. Chen, Z. H., Akin, B. L., Stokes, D. L., and Jones, L. R. (2006) Cross-linking of C-terminal residues of phospholamban to the Ca^{2+} pump of cardiac sarcoplasmic reticulum to probe spatial and functional interactions within the transmembrane domain. *J. Biol. Chem. 281*, 14163–14172.
29. Hughes, E., and Middleton, D. A. (2003) Solid-state NMR reveals structural changes in phospholamban accompanying the functional regulation of Ca^{2+}-ATPase. *J. Biol. Chem. 278*, 20835–20842.
30. Kirby, T. L., Karim, C. B., and Thomas, D. D. (2004) Electron paramagnetic resonance reveals a large-scale conformational change in the cytoplasmic domain of phospholamban upon binding to the sarcoplasmic reticulum Ca-ATPase. *Biochemistry 43*, 5842–5852.
31. Mueller, B., Karim, C. B., Negrashov, I. V., Kutchai, H., and Thomas, D. D. (2004) Direct detection of phospholamban and sarcoplasmic reticulum Ca-ATPase interaction in membranes using fluorescence resonance energy transfers. *Biochemistry 43*, 8754–8765.
32. Hutter, M. C., Krebs, J., Meiler, J., Griesinger, C., Carafoli, E., and Helms, V. (2002) A structural model of the complex formed by phospholamban and the calcium pump of sarcoplasmic reticulum obtained by molecular mechanics. *ChemBioChem 3*, 1200–1208.
33. Pollesello, P., Annila, A., and Ovaska, M. (1999) Structure of the 1–36 amino-terminal fragment of human phospholamban by nuclear magnetic resonance and modeling of the phospholamban pentamer. *Biophys. J. 76*, 1784–1795.
34. Zamoon, J., Nitu, F., Karim, C., Thomas, D. D., and Veglia, G. (2005) Mapping the interaction surface of a membrane protein: Unveiling the conformational switch of phospholamban in calcium pump regulation. *Proc. Natl. Acad. Sci. U.S.A. 102*, 4747–4752.
35. Saito, H. (1986) Conformation-Dependent ^{13}C Chemical Shifts—A new means of conformational characterization as obtained by high-resolution solid-state ^{13}C NMR. *Magn. Reson. Chem. 24*, 835–852.
36. Luca, S., White, J. F., Sohal, A. K., Filippov, D. V., van Boom, J. H., Grisshammer, R., and Baldus, M. (2003) The conformation of neurotensin bound to its G protein-coupled receptor. *Proc. Natl. Acad. Sci. U.S.A. 100*, 10706–10711.
37. Douglas, J. L., Trieber, C. A., Afara, M., and Young, H. S. (2005) Rapid, high-yield expression and purification of Ca^{2+}-ATPase regulatory proteins for high-resolution structural studies. *Protein Expression Purif. 40*, 118–125.
38. Eletr, S., and Inesi, G. (1972) Phospholipid orientation in sarcoplasmic membranes—Spin-label ESR and proton NMR studies. *Biochim. Biophys. Acta 282*, 174–179.
39. Stokes, D. L., and Green, N. M. (1990) Three-dimensional crystals of CaATPase from sarcoplasmic reticulum. Symmetry and molecular packing. *Biophys. J. 57*, 1–14.
40. Warren, G. B., Toon, P. A., Birdsall, N. J., Lee, A. G., and Metcalfe, J. C. (1974) Reconstitution of a calcium-pump using defined membrane components. *Proc. Natl. Acad. Sci. U.S.A. 71*, 622–626.
41. Hohwy, M., Rienstra, C. M., Jaroniec, C. P., and Griffin, R. G. (1999) Fivefold symmetric homonuclear dipolar recoupling in rotating solids: Application to double quantum spectroscopy. *J. Chem. Phys. 110*, 7983–7992.
42. Bloembergen, N. (1949) On the interaction of nuclear spins in a crystalline lattice. *Physica 15*, 386–426.
43. Suter, D., and Ernst, R. R. (1982) Spectral spin diffusion in the presence of an extraneous dipolar reservoir. *Phys. Rev. B: Condens. Matter Mater. Phys. 25*, 6038–6041.
44. Seidel, K., Lange, A., Becker, S., Hughes, C. E., Heise, H., and Baldus, M. (2004) Protein solid-state NMR resonance assignments from (^{13}C,^{13}C) correlation spectroscopy. *Phys. Chem. Chem. Phys. 6*, 5090–5093.
45. Baldus, M. (2002) Correlation experiments for assignment and structure elucidation of immobilized polypeptides under magic angle spinning. *Prog. Nucl. Magn. Reson. Spectrosc. 41*, 1–47.
46. Baldus, M., Petkova, A. T., Herzfeld, J., and Griffin, R. G. (1998) Cross polarization in the tilted frame: Assignment and spectral simplification in heteronuclear spin systems. *Mol. Phys. 95*, 1197–1207.
47. Takegoshi, K., Nakamura, S., and Terao, T. (2001) $^{13}C-^{1}H$ dipolar-assisted rotational resonance in magic-angle spinning NMR. *Chem. Phys. Lett. 344*, 631–637.
48. Morris, G. A., and Freeman, R. (1979) Enhancement of nuclear magnetic resonance signals by polarization transfer. *J. Am. Chem. Soc. 101*, 760–762.
49. Baldus, M., and Meier, B. H. (1996) Total correlation spectroscopy in the solid state. The use of scalar couplings to determine the through-bond connectivity. *J. Magn. Reson. A 121*, 65–69.

50. Fung, B. M., Khitrin, A. K., and Ermolaev, K. (2000) An improved broadband decoupling sequence for liquid crystals and solids. *J. Magn. Reson. 142*, 97–101.
51. Shaka, A. J., Barker, P. B., and Freeman, R. (1985) Computer-optimized decoupling scheme for wideband applications and low-level operation. *J. Magn. Reson. 64*, 547–552.
52. Seavey, B. R., Farr, E. A., Westler, W. M., and Markley, J. L. (1991) A relational database for sequence-specific protein NMR data. *J. Biomol. NMR 1*, 217–236.
53. Brunger, A. T., Adams, P. D., Clore, G. M., DeLano, W. L., Gros, P., Grosse-Kunstleve, R. W., Jiang, J. S., Kuszewski, J., Nilges, M., Pannu, N. S., Read, R. J., Rice, L. M., Simonson, T., and Warren, G. L. (1998) Crystallography and NMR system: A new software suite for macromolecular structure determination. *Acta Crystallogr., Sect. D: Biol. Crystallogr. 54*, 905–921.
54. Dominguez, C., Boelens, R., and Bonvin, A. (2003) HADDOCK: A protein−protein docking approach based on biochemical or biophysical information. *J. Am. Chem. Soc. 125*, 1731–1737.
55. Berman, H. M., Westbrook, J., Feng, Z., Gilliland, G., Bhat, T. N., Weissig, H., Shindyalov, I. N., and Bourne, P. E. (2000) The Protein Data Bank. *Nucleic Acids Res. 28*, 235–242.
56. Wang, Y. J., and Jardetzky, O. (2002) Probability-based protein secondary structure identification using combined NMR chemical-shift data. *Protein Sci. 11*, 852–861.
57. Takahashi, M., Kondou, Y., and Toyoshima, C. (2007) Interdomain communication in calcium pump as revealed in the crystal structures with transmembrane inhibitors. *Proc. Natl. Acad. Sci. U.S.A. 104*, 5800–5805.
58. Olesen, C., Picard, M., Winther, A. M. L., Gyrup, C., Morth, J. P., Oxvig, C., Moller, J. V., and Nissen, P. (2007) The structural basis of calcium transport by the calcium pump. *Nature 450*, 1036–1042.
59. Li, J. H., Boschek, C. B., Xiong, Y. J., Sacksteder, C. A., Squier, T. C., and Bigelow, D. J. (2005) Essential role for Pro^{21} in phospholamban for optimal inhibition of the Ca-ATPase. *Biochemistry 44*, 16181–16191.
60. MacLennan, D. H., Abu-Abed, M., and Kang, C. (2002) Structure−function relationships in Ca^{2+} cycling proteins. *J. Mol. Cell. Cardiol. 34*, 897–918.

BI7024194